Editorial Manager(tm) for Annals of Biomedical Engineering
Manuscript Draft

Manuscript Number:

Title: Hemodynamic performance of stage-2 univentricular reconstruction: Glenn vs. hemi-Fontan templates

Article Type: Research Article

Section/Category:

Keywords: CFD, Patien-Specific, Fontan, Congenital, Univentricular, PIV, Hemodynamics

Corresponding Author: Kerem Pekkan, PhD

Corresponding Author's Institution: Carnegie Mellon University

First Author: Kerem Pekkan, PhD

Order of Authors: Kerem Pekkan, PhD; Lakshimi P Dasi, PhD; Diane de Zélicourt, MS; Kartik S Sundareswaran, MS; Mark A Fogel, MD; Kirk R Kanter, MD; Ajit P Yoganathan, PhD

Manuscript Region of Origin:

Abstract: Flow structures, hemodynamics and the hydrodynamic surgical pathway resistances of the final stage functional single ventricle reconstruction, namely the total cavopulmonary connection (TCPC) anatomy, have been investigated extensively. However, the second stage surgical anatomy (i.e. bi-directional Glenn or hemi-Fontan template) has received little attention. Towards a complete physiological understanding that spans all the three stages of Fontan reconstruction process, a multi-faceted study is initiated involving; magnetic resonance imaging (MRI), phase contrast MRI, computational and experimental fluid dynamics methodologies. Parametric idealized (n=6), patient specific (n=7) and their virtual surgery variant (n=7) computer and rapid prototype three-dimensional models of 2nd stage TCPC anatomies were created (total n=20). Patient specific models, hemi-Fontan (n=3) and Glenn (n=3), all models having approximately similar cavopulmonary size and PA diameter, enabled a quantitative hemodynamic comparison of the two contemporary second stage Fontan templates. Results in patient specific and idealized models showed that the Glenn connection template is hemodynamicaly more efficient with (83%

p=0.08 in patient specific models and 66% in idealized models) lower power losses compared to hemi-Fontan template respectively due to its direct end-to-side anastomosis. Relative influence of secondary surgical features like hemi-Fontan pouch size, pouch stenosis, flare and branch stenosis are quantified through free-formed deformed, virtual surgery anatomical models. Among those geometrical features SVC anastomosis stenosis and branch stenosis is found to be the most critical parameters in increasing the power loss. The pouch size and flare shape is found to be less significant. Compared to the third stage surgery the hydrodynamic resistance of the 2nd stage is considerably lower (both in idealized models and in anatomical models at MRI resting conditions) than the third stage surgery for both hemi- and Glenn templates. These results can impact the surgical design and planning of the staged TCPC reconstruction.

Hemodynamic performance of stage-2 univentricular reconstruction: Glenn vs. hemi-Fontan templates

Kerem Pekkan[1], Lakshimi P. Dasi[2], Diane de Zélicourt[2], Kartik S. Sundareswaran[2], Mark A. Fogel[3], Kirk R. Kanter[4], Ajit P. Yoganathan[2]

[1]Department of Biomedical Engineering, Carnegie Mellon University, PA, USA, [2]Wallace H. Coulter Department of Biomedical Engineering, Georgia Institute of Technology, GA, USA, [3]Children's Hospital of Philadelphia, PA, USA , [4] Department of Cardiothoracic Surgery, Emory University School of Medicine, Atlanta, GA

Running title: Hemodynamics of Glenn vs. hemi-Fontan

Address for Correspondence:
Ajit P. Yoganathan, Ph.D.
Wallace H. Coulter School of Biomedical Engineering
Georgia Institute of Technology
Room 2119 U.A. Whitaker Building, 313 Ferst Dr.
Atlanta, GA 30332-0535
Phone: (404) 894-2849
Fax no: (404) 385 - 5013
e-mail: ajit.yoganathan@bme.gatech.edu

Abstract

Flow structures, hemodynamics and the hydrodynamic surgical pathway resistances of the final stage functional single ventricle reconstruction, namely the total cavopulmonary connection (TCPC) anatomy, have been investigated extensively. However, the second stage surgical anatomy (i.e. bi-directional Glenn or hemi-Fontan template) has received little attention. Towards a complete physiological understanding that spans all the three stages of Fontan reconstruction process, a multi-faceted study is initiated involving; magnetic resonance imaging (MRI), phase contrast MRI, computational and experimental fluid dynamics methodologies. Parametric idealized (n=6), patient specific (n=7) and their virtual surgery variant (n=7) computer and rapid prototype three-dimensional models of 2nd stage TCPC anatomies were created (total n=20). Patient specific models, hemi-Fontan (n=3) and Glenn (n=3), all models having approximately similar cavopulmonary size and PA diameter, enabled a quantitative hemodynamic comparison of the two contemporary second stage Fontan templates. Results in patient specific and idealized models showed that the Glenn connection template is hemodynamicaly more efficient with (83% p=0.08 in patient specific models and 66% in idealized models) lower power losses compared to hemi-Fontan template respectively due to its direct end-to-side anastomosis. Relative influence of secondary surgical features like hemi-Fontan pouch size, pouch stenosis, flare and branch stenosis are quantified through free-formed deformed, virtual surgery anatomical models. Among those geometrical features SVC anastomosis stenosis and branch stenosis is found to be the most critical parameters in increasing the power loss. The pouch size and flare shape is found to be less significant. Compared to the third stage surgery the hydrodynamic resistance of the 2nd stage is considerably lower (both in idealized models and in anatomical models at MRI resting conditions) than the third stage surgery for both hemi- and Glenn templates. These results can impact the surgical design and planning of the staged TCPC reconstruction.

1. Introduction

The incidence of children born with a single ventricle congenital heart defect in which there is only one effective pumping chamber is about 2 per 1000 births (or about 2000 in a year in the US). Surgical repairs that separate the pulmonary and systemic circuits, placing them in series with the univentricular pump, termed "Fontan Repairs," are palliative, and unfortunately not curative [1, 2]. Operations are routinely staged (three stages) over many years and survivors often require a lifetime (rather limited) of intensive medical attention [3, 4].

Since its introduction in 1971 by Fontan et.al [5], the right heart by-pass surgeries have evolved towards optimal hydrodynamic pathway designs (atrio-pulmonary to extracardiac Fontan and recently the bifurcated IVC) [6, 7]. Based on the several clinical, *in vivo* and *in vitro* flow studies [8], two contemporary surgical templates, namely intra-atrial lateral tunnel and extra-cardiac TCPC are now the current final-stage (S3R) surgical procedures of choice [9-11]. The hemodynamic advantage of one surgical template type over the other is a critical long-asked clinical question [12, 13]. However a definite conclusion is challenged due to the spectrum of downstream/upstream, coexistent, patient-to-patient variable vascular factors (including univentricle heart function [14], pulmonary, hepatic venous physiology, respiratory pump) and the anatomical and physiological variability of congenital heart defects. Recently through a large number of patient-specific *in vitro* TCPC models a statistically significant hemodynamic comparison of the intra-atrial vs. extra-cardiac TCPC templates was made possible [15]. The quality of hepatic flow distribution [16], anatomical features [17] and *in vivo* flow structures [18] also presented significant differences between these templates.

Likewise the hemodynamic basis of surgical template preference for the second stage palliation (S2R) is obscure where either a Glenn [19] or a hemi-Fontan [20-22] type SVC

anastomosis is the current procedure of choice, Fig 1. The decision of one template type over the other is mainly left to the surgeon's discretion which is primarily based on the former training and experience. 2nd stage template type is possibly critical as in all cases it poses constraints to the final-stage template as well. A hemi-Fontan connection should be followed by an intra-atrial (or lateral tunnel) type Fontan due to the placement of the atrial patch. Whereas Glenn type 2nd stage template allows both of the two contemporary options for the last stage surgery in which either an intra-atrial or an extra-cardiac type TCPC connection can be created. Second stage surgeries of bilateral SVC always require one Glenn anastomosis at the right SVC. Studies focusing the quantitative hemodynamics and comparative flow dynamics of these surgical templates are limited. To the authors knowledge Glenn and hemi-Fontan 2nd stage templates are compared only in a single study [23] which favored the hemi-Fontan type connection for the 2nd stage, based on the CFD results of only a single hybrid idealized/anatomical model. Our recent cohort of multi-institute MRI NIH-congenital heart disease morphology database provided an opportunity to revisit the hemi-Fontan vs. Glenn hemodynamic performance comparison from a neutral perspective and more importantly comprehensively using several patient-specific models.

In order to improve the hemodynamic efficiency of the surgical repair site a large volume of modeling studies both with idealized (earlier) and patient-specific models (more recently) have been performed [24]. The biggest challenge in patient-specific modeling is the co-existence of secondary morphological features (like branch stenosis, vessel volume and pouch size) which influence the fluid flow performance and preclude any conclusions on the TCPC pathway itself. Maintaining a large sample size as employed in our recent study [15] through an efficient computational pipeline [25] may overcome this challenge. An alternative analysis approach is utilizing the recent "virtual" surgery tools [26-29] where the influencing secondary anatomical

features can be selectively removed from the 3D reconstruction and the associated changes in hemodynamics can be evaluated quantitatively [28]. The present study which introduces the quantitative three-dimensional fluid dynamics of 2nd stage templates in multiple patient-specific models first time in the literature, utilizes idealized models, multiple anatomical models and "virtual" surgeries, therefore employs all available quantitative tools towards an unbiased conclusion.

Recent quantitative investigations on univentricle circulation using lumped parameter models highlighted the importance of venous inflow parameters on cardiac output [30-32]. Reasons behind the chronic venous compliance remodeling (up to 400%) [33] and acute post-op venous blood volume shift are clarified through these models [32]. Governed by the Guytonian venous characteristics [34, 35], single ventricle cardiac output is highly sensitive to the pulmonary vascular resistance (PVR) [36], which is located downstream of the venous compliance. Hemodynamic influence of the TCPC surgical pathway resistance, in series to the lungs, and comparable in magnitude to the PVR (Typical values are provided in Ref. [37] and Ref. [32]) is similar to the effect of pulmonary vascular resistance as pictured by Guyton's isolated venous theory [38, 39]. Our recent calculations showed that the sensitivity of cardiac output to the pulmonary vascular resistance is -0.064 and -0.88 for normal and univentricle circulations respectively [36]. While the hydrodynamic resistance of the final stage TCPC surgery is extensively characterized in our previous studies [32, 37], the second stage reconstructions have not been studied and their surgical pathway hydrodynamic resistance is still unknown. Its value relative to the PVR is important for understanding the physiology of second stage surgery, to optimize fluid flow and to highlight the physiological differences of S2R from S3R.

2. Methodology

Methodology employed in this work has been described extensively in our earlier publications and should be referred for details. The reader should visit Ref. [40-42] for anatomical segmentation and 3D reconstruction, Ref. [43] for rapid-prototyping of the physical *in vitro* anatomical model, Ref [18, 44, 45] for MRI velocity acquisition , Ref. [46-48] for *in vitro* tests and Ref. [28, 37, 49, 50] for computational fluid dynamics (CFD) modeling. Only parameters specific to the hemi- and Glenn anatomies will be presented here. Particularly the required CFD verification and validation tests for the 2nd stage anatomies are completed since the 2nd stage surgical anatomies are morphologically different than the 3rd stage TCPC (even though they bear a simpler topology, with only three branches). For CFD veification purposes secondary downstream/upstream anatomical features like distal PA bending and 3D reconstruction smoothing influencing the power loss (PL) predictions are investigated as well in the Appendix.

2.1. Patient specific anatomies

The multi-center NIH Fontan patient MRI database has been extended to study the anatomic elements of the 2nd stage TCPC reconstruction (n = 220 and n = 70 for S3R and S2R respectively as of October 2007). Informed consent was obtained and all associated studies were approved by the Internal Review Boards of the Children's Hospital of Philadelphia, the Children's Healthcare of Atlanta, the University of North Carolina, and the Georgia Institute of Technology. 6 models (3 from each set of hemi or Glenn reconstruction) is selected based on the following criteria: Existence of complete PC-MRI flow information, no apparent branch stenosis, relatively similar pulmonary artery cross-sectional area, similar connection volume and the existence of the 3rd stage Fontan anatomy (to be used in future studies). In addition to this set, a typical Glenn model is selected (Database ID: CHOA013) from the database to be used in the virtual surgery suite (See

Section 2.2) which has moderate stenosis in both PA branches with a distinct bifurcating anastomosis pathway morphology.

The anatomical models are obtained from patient MRI data by enhancing the out-of-plane image resolution using an adaptive control grid interpolation technique then segmenting the vessels of interest. These models are reconstructed to be used in CFD studies and the corresponding transparent rapid prototypes are manufactured for use in the particle image velocimetry (PIV) studies, Fig 2.

2.2. Virtual surgeries and computer-aided anatomy editing

For a systematic quantitative investigation of the effects of certain anatomical surgical features (like branch stenosis, pouch size or flare) an in-house virtual anatomy editing tool is employed [26, 27, 51]. The present version this tool allow the user to free-form deform the MRI reconstructions in the computer, thus allowing the realization of "virtual" surgery concept [28, 47] very efficiently. Any number of 3D reconstructions (heart, aorta, veins, IVC and 2^{nd} stage anatomy) can be assembled together to identify surgical constraints [51]. The extend of anatomical modifications performed on the patient-specific anatomies by the user are quantified by the skeletization and geometrical characterization tools [17].

Unit anatomy editing operations (changing connection shape and adding a flare) are performed in both of the 2^{nd} stage templates (Glenn, Database ID: CHOA013 and hemi-Fontan, Database ID: CHOP036) making a total of 4 new derived 3D morphologies. Whereas the effect of stenosis is studied only in the Glenn model (Database ID: CHOA013) where two RPA and one LPA stenosis are sequentially dilated in the computer (3 new derived models).

2.3. PC-MRI Acquisition and Analysis

The study utilized a Siemens 1.5 Tesla whole body MRI scanner for the acquisition of patient specific boundary conditions. Retrospectively-triggered, through-plane, phase-encoded velocity mapping was performed on a plane perpendicular to the flow in the ascending aorta positioned approximately 2 mm above the aortic valve. The velocity encoding used was ± 150 cm/s. The effective repetition time was 20 ms, which yielded 30 cardiac phases, the echo time was 2.5 ms and the image matrix size was 128 x 256 pixels. The field of view was about 30 mm and a rectangular field of view was used. The slice thickness was 5 mm. The caval and pulmonary branch cross-sections were then semi-automatically segmented using a gradient based active contour scheme and flow was quantified throughout the cardiac cycle.

2.4. Idealized models with parametric dimensions

Idealized models, with parametric dimensions, representing the pre-surgery state of the standard 13.335 mm diameter one-diameter offset model [7, 52-54] is created in the computer aided design software Proengineer (PTC Inc, Needham, MA, USA). Four idealized models are employed in this study to investigate the effects of SVC offset with varying degrees (0 to 13.335 mm) with respect to the PA centerline, Fig 3. Zero-offset model corresponds to a typical Glenn shunt. For larger SVC offset values, there is a danger and possibility of generating an SVC pouch stenosis located at the side-to-side anastomosis region (which is reported to be clinically significant, 1.5% [55]). The effect of this constriction type on flow dynamics is studied in two idealized parametric models with varying degrees of pouch orifice cross-sectional diameter (6 to 10 mm), Fig 3.

2.5. Numerics

2.5.a. Grid generation

High-quality tetrahedral grids are generated using GAMBIT (Fluent Inc., Lebanon, NH) for both idealized and anatomical models. For the baseline idealized 2nd Stage model (Model GL) and for CHOP036 computational grids with different refinement levels are created for verification purposes (Sections 3.1 and 3.3). The parameters used in grid generation, are summarized in Table 1. To achieve good convergence strict mesh quality checks are performed.

2.5.b. CFD solver settings

For all models, flow fields were computed by solving the three-dimensional steady, incompressible Navier-Stokes equations using the commercial CFD solver FIDAP (Fluent Inc., Lebanon, NH) with rigid vessel walls [37]. Blood was assumed incompressible and Newtonian, which is consistent with previous experimental and numerical studies ($\rho = 1060 kg \cdot m^{-3}$, $\mu = 3.5 \times 10^{-3} Pa \cdot s$).

2.5.c. Boundary conditions

For anatomical models, simulations are performed at the resting PC-MRI flow rates which are specified as plug-flow velocity inflow boundary conditions at 9-diameter extended outlets and inlets. Table 2 summarizes the boundary conditions used in CFD simulations. For idealized models, 40% [56] of our standard cardiac output value of 4 LPM [28, 44] is specified from the SVC. Idealized models also feature extended outlets and inlets but at outlets pressure boundary conditions are specified. Outflow velocity and pressure boundary conditions are tested and found

to be equivalent in earlier studies [50]. The convergence criterion was set to 10E-4 for all degrees-of-freedom.

2.6. Particle Image Velocimetry

Digital particle image velocimetry measurements were two models (1 hemi and 1 Glenn) at in vivo cardiac output and and 50-50 PA splits. We used a LaVision system (LaVision GmbH, Germany), which included a data acquisition software package (DaVis-Flowmaster), two 17mJ miniYag lasers (λ = 514nm) and one camera. In order to increase image quality, fluorescent Rhodamine B particles (MF/RhB, size range: 2.5 to 5 μm, Microparticles GmbH, Berlin, Germany) were used to seed the flow. For the second stage anatomies only changes in the in vitro experimental set up and measurement technique, as described earlier [47, 48], were the elimination of vena cava (IVC) piping for all models and the addition of LSVC pipe for Chop53. The laser sheet optical pathway mechanism is also redesigned so that it can be traversed throughout the model more efficiently.

3. Results

3.1. Idealized models

Hydrodynamic power loss values at different pulmonary flow splits are calculated from the CFD results for all idealized models and plotted in Fig 4a and 4b. The hydrodynamic power loss of model GL is lower for all the hemi-Fontan models. Larger SVC offsets increase the power loss even further. The GL model power loss is 16 %, 26 %, and 62 % lower compared to HM-1, HM-2 and HM-3 respectively (the three hemi-Fontan models with different degrees of SVC offset). Compared to the earlier power loss results of the idealized third stage (S3R) one-diameter-offset

TCPC model (~5.6mW) [28, 54], second stage power losses are considerably lower (~1.9mW for HM-3) (~66 % lower for HM-3).

Effect of anastomosis stenosis on hydrodynamic power loss is presented in Figure 4b. Hydrodyanamic power loss is significantly more sensitive to the anastomosis stenosis than the SVC offset parameter. Larger stenosis diameters caused considerably larger power losses in the second stage cavopulmonary connection, Fig 4b. (1.9, 2.4 and 7.3 mW for HM-3, HM-5 and HM-6 respectively)

At the pulmonary branches swirling flow is observed in all models, Fig 5. Unlike the PA swirl characteristics of the final stage TCPC, the second stage had only a single swirl structure (vortex) at each PA. A relatively minor swirling flow structure at the pouch region is also noticed. SVC anastomosis created jet-like flow in the connection which stagnates and bifurcates at the PA lateral wall, Fig 5.

Grid verification study is performed for the idealized Glenn anatomy (GL). Models with four different grid (computational mesh) densities (79929, 242070, 406186 and 553686 elements) are created which resulted 14.8 %, 9.5% and 1.4% differences in Power Loss compared to the finest grid size model respectively. Flow fields for all models are qualitatively similar. The mesh density corresponding to the 406186 elements (resulting 1.4% difference) is maintained in all idealized models.

3.2. Experimental validation

Experimental validation of the second stage TCPC CFD model for the patient-specific anatomical models is an essential task and performed by comparing flow fields obtained from CFD and particle image velocimetry. Figure 6a, and 6b shows the comparison of computed vector fields with the measured velocity field using PIV in one slice of hemi (CHOP072) and Glenn (CHOP057) model respectively. As seen, the computational scheme successfully captured the topology of flow structures through both these models. However, we acknowledge here a mismatch between velocity magnitudes in certain regions of the measurement plane and attribute this to the fully developed forcing at the inlets of these models in the computational scheme and PIV missing some flow vectors due to poor laser illumination. Fully developed flow at the inlet of these models was not observed from the measured fields (very difficult to control experimentally due to small vessel sizes and circular pipe connections) and is attributed to the elliptic nature of the governing equations.

3.3. Anatomical models – Flow structures and power loss

For the six second stage patient specific models the calculated power loss values are tabulated in Table 2 with other major determinants of power loss (PA diameter, model size, SVC flowrate). Average power loss for the three Glenn models is 83% lower than the three hemi-Fontan models. The p Value for PL hemi > PL Glenn is 0.08, which is near significant considering such a low sample size and the inclusion of a bilateral model. The test used was 2-sample unpaired Mann Whitney Non parametric Test. The same test for the other major determinants like RPA diameter Glenn vs. RPA diameter hemi-Fontan gives a p value of 1.0.

We have visualized the pressure and flow fields in Glenn and hemi-Fontan models with alternating color streamline technique (Supplementary Material of Ref. [37]) in Fig 7 and 8 respectively. Flow fields in Glenn models are found to be more uniform and bifurcated without any recirculation to the pulmonary arteries. Only exception is CHOP057 where the RPA stream went into the LPA branch before flowing back to the left lung. hemi-Fontan models with large pouches featured very complex swirling flow structures at the connection and in both PA (preferably at LPA) branches, Fig 8. Well-defined stagnation flow pressure fields, with increasing pressure values) at the connection region are observed in Glenn models, Fig 7 (This potential energy is converted to the kinetic energy in the accelerating PA flow). Pressure drop in hemi-Fontan models are larger compared to the Glenn models.

A grid verification study is performed for the hemi-Fontan model (Database ID: CHOP036). CFD models with three grid sizes 133936, 232036 and 330555 are created which resulted 3.4% and 1.5% differences (compared to the finest grid size) in Power Loss respectively. Flow fields obtained with all grid sizes were similar as shown in Fig 9.

3.4. Relative influence of morphological features

For the original and “virtual” surgically modified anatomies calculated three dimensional flow streamlines are plotted in Fig 10. The original hemi-Fontan and Glenn models used in this study are CHOP036 and CHOA013 respectively. In spite of the differences in flow streamlines, virtual modifications of the connection region produced little variation in hydrodynamic power loss for both Glenn (CHOA013 to Model-A in Fig 9) and hemi-Fontan templates (CHOP036 to Model-G in Fig 9). Creating a flatter PA bifurcation (larger connection size) in the Glenn model (Model-A)

produced 8.6% decrease in the power loss. While in the hemi-Fontan model pouch size reduction (Model-G) produced only 6.6 % increase in average power loss.

Addition of a large virtual LPA flare to both hemi-Fontan (CHOP036 to Model-H in Fig 9) and Glenn models (Model-C to Model-D in Fig 9) produced insignificant changes in the power loss characteristics.

Two RPA and one LPA branch stenosis of the Glenn (CHOA013) model is virtually dilated one-by-one which resulted significant differences in power loss values. Proximal RPA stenosis dilation (Model-A to Model-B in Fig 9) produced 13%, distal RPA stenosis dilation (Model-B to Model-C in Fig 9) produced an additional 34% and the discrete LPA stenosis dilation (Model-D to Model-E in Fig 9) produced an additional 70% decrease in average power loss values.

4. Discussion

A large-scale modeling attempt involving 18 different patient-specific S2R morphologies and 6 idealized models to quantify the hemodynamic differences between hemi- and Glenn type surgical pathways is presented. This study contributed to the earlier understanding which was based on a single idealized/anatomical model [57]. Using a large number of anatomical models and the recent virtual “anatomy editing” tool the significant hemodynamic differences between the two surgical pathways and the sensitivity of hydrodynamic performance to the major anatomical features are quantified. Among the pouch shape, flare size, caval confluence, PA bifurcation and branch diameters, the last two geometrical features are found to be most significant in influencing the hydrodynamic loss. The importance of 3D caval inlet orientation have been highlighted extensively in the earlier reports for S3R and found to be equally important for S2R as well. Effect

of 3D reconstruction smoothing in relatively smaller S2R models compared to the S3R on the power loss results of the S2R is also visited in the Appendix for verification purposes.

The “most optimal” S3R pathway design that can be realized is different for the hemi- and Glenn type anastomosis and requires an extensive modeling study involving pre- and post-op MRI scans of several patients. While efforts for such a study are underway, for the idealized S2R models of this manuscript we completed the Fontan palliation in the computer and verified that the SVC offset of the hemi-Fontan remains to be a factor for increasing the S3R power losses (with similar percentage) as well. However S3R introduces additional secondary influencing factors [58] and therefore we strongly believe that such optimization studies should be customized for each patient based on the preoperative MRI anatomy via the CFD tools.

In spite of being a temporary time-point in staged palliation, hydrodynamic performance at the 2nd stage post-op is critical for understanding the physiology of the univentricular circulation. Characteristics of the pathway hemodynamics at this stage will provide important data for lumped parameter models, singe ventricle heart function and PA growth studies. Due to the unaltered inferior venous return the effect of hydrodynamic power loss on cardiac output at this stage should be relatively minor. Studies that target further improvements should focus on SVC venous return and head-neck perfusion balance. Likewise for a typical leg exercise pattern (only increasing the IVC flow rate) the S2R pathway resistance is less significant for the exercise performance compared to the lower oxygen saturation of second stage. The pathway resistance values for the S2R are found to be considerably lower compared to the typical values of the S3R. This is mostly attributable to the lower cardiac output that runs through the S2R surgical pathway (SVC return in the idealized models were kept higher in this study (1.6LPM) compared to the anatomical set (~1LPM) to be compatible with the earlier S3R one-diameter offset idealized model studies).

Power loss variation for different PA splits for S2R was also found to be flatter compared to the S3R characteristics. These results enable quantitative comparison of the hydrodynamic factors as a major determinant of the single ventricle physiology.

A few limitations of this *in vitro* study should be mentioned. First, this study was conducted using steady inflow conditions. Changing the inflow conditions to unsteady patient-specific ones will most likely alter the observed flow structures and associated power losses. Variation of power loss over the cardiac cycle is critical. However for the S2R stage, having a single SVC inlet, the mean flow is adequate for comparing the hydrodynamic performance at different time-points. Factors such as the intra-thoracic pressure variations due to breathing, diaphragm and heart motion, which are known to induce significant unsteadiness into the single-ventricle venous flow, should ultimately be alleviated. For example, detailed pulmonary characteristics can be modeled as demonstrated recently giving the information at a single pulmonary split while present analysis methodology quantifies the pathway performance for multiple PA split conditions. In addition, this study assumes the vessel walls to be rigid. Numerical simulations with flexible walls have recently been presented by Masters et al [59]. and DeGroff [60] for idealized TCPC geometries. However, relieving these assumptions in patient-specific geometries will require the development of fast 3D reconstruction algorithms that spans all CMRI phases and high-resolution CFD solvers which are ongoing and planed for future communications.

5. Conclusions

This study investigated the pathway hemodynamics of two contemporary second stage palliation templates (Glenn and hemi-Fontan) through multiple quantitative analysis tools (idealized models, patient-specific models, virtual surgeries and experimental fluid dynamics). Through these

analyses a Glenn type anastomosis is favorable compared to hemi-Fontan based on solely the hemodynamic parameters and 3D fluid dynamic performance. Other clinical factors and surgeons/cardiologists judgment based on the condition of individual patient is equally important for deciding the best template and achieving optimal outcome. The clinical validation of one template over the other is challenging which will ultimately require prospective testing in Fontan patients. For both template types, the hydrodynamic power loss of the second stage pathway is considerably lower than the final completed TCPC.

Appendix

Effects of secondary morphological features on hydrodynamic power loss

The effects of secondary and peripheral anatomical features on the computed TCPC power loss values (S3R) have been well established in the earlier verification studies. This communication is an appropriate place to summarize these briefly for the S2R. These factors should influence the computed fluid dynamics of both Glenn and hemi-Fontan models more-or-less in the same magnitude thus should not influence the stated conclusions of this manuscript. The effect of the extra 3D reconstruction smoothing has studied in the Glenn model (CHOA030), Fig A1. Calculated power loss values are -0.250 mW and -0.277 mW with our standard reconstruction protocol and with the extra surface smoothed model respectively. The effect of PA branch length and proximal bending is studied in another Glenn model (CHOP057), Fig A2. As expected the PA bending increased the power loss values from 0.044 mW to 0.045 mW which was negligible for this configuration. For all other models morphology of the PA branches are relatively straight with gentler radius of curvatures.

Acknowledgements

This work was supported by a grant from the National Heart, Lung, and Blood Institute, HL67622. We also acknowledge Dr. Dave Frakes for providing the ACGI technology and Dr. Hiroumi Kitajima for processing some of the patient MRI datasets. Experimental and computational studies are made possible with the help of our brilliant undergraduate students: Vasu Yernini, Maria Restrepo, Kiyu Kim and Quantez Freeman.

References

[1] de Leval, M., 1988, "The Fontan circulation: What have we learned? What to expect?," Pediatr Cardiol., 19(4), pp. 316-320.

[2] de Leval, M., 2005, "The Fontan circulation: a challenge to William Harvey?," Nat Clin Pract Cardiovasc Med., 2(4), pp. 202-208.

[3] Mitchell, M. E., Ittenbach, R. F., Gaynor, J. W., Wernovsky, G., Nicolson, S., and Spray, T. L., 2006, "Intermediate outcomes after the Fontan procedure in the current era," The Journal of Thoracic and Cardiovascular Surgery, 131(1), pp. 172-180.

[4] Fontan, F., Kirklin, J. W., Fernandez, G., Costa, F., Naftel, D. C., Tritto, F., and Blackstone, E. H., 1990, "Outcome after a "perfect" Fontan operation," Circulation, 81(5), pp. 1520-1536.

[5] Fontan, F., and Baudet, E., 1971, "Surgical repair of tricuspid atresia," Thorax, 26(3), pp. 240-248.

[6] de Leval, M. R., Kilner, P., Gewillig, M., and Bull, C., 1988, "Total cavopulmonary connection: a logical alternative to atriopulmonary connection for complex Fontan operations. Experimental studies and early clinical experience," J Thorac Cardiovasc Surg, 96(5), pp. 682-695.

[7] Soerensen, D. D., Pekkan, K., de Zelicourt, D., Sharma, S., Kanter, K., Fogel, M., and Yoganathan, A. P., 2007, "Introduction of a new optimized total cavopulmonary connection," Ann Thorac Surg, 83(6), pp. 2182-2190.

[8] Giroud, J. M., and Jacobs, J. P., 2006, "Fontan's operation: evolution from a procedure to a process," Cardiol Young, 16 Suppl 1, pp. 67-71.

[9] Kumar, S. P., Rubinstein, C. S., Simsic, J. M., Taylor, A. B., Saul, J. P., and Bradley, S. M., 2003, "Lateral tunnel versus extracardiac conduit fontan procedure: a concurrent comparison," The Annals of Thoracic Surgery, 76(5), pp. 1389-1397.

[10] Stamm, C., Friehs, I., Mayer, J. E., Zurakowski, D., Triedman, J. K., Moran, A. M., Walsh, E. P., Lock, J. E., Jonas, R. A., and del Nido, P. J., 2001, "Long-term results of the lateral tunnel Fontan operation," Journal of Thoracic and Cardiovascular Surgery, 121(1), pp. 28-41.

[11] Azakie, A., McCrindle, B. W., Van Arsdell, G., Benson, L. N., Coles, J., Hamilton, R., Freedom, R. M., and Williams, W. G., 2001, "Extracardiac conduit versus lateral tunnel cavopulmonary connections at a single institution: Impact on outcomes," Journal of Thoracic and Cardiovascular Surgery, 122(6), pp. 1219-1228.

[12] Fiore, A. C., Turrentine, M., Rodefeld, M., Vijay, P., Schwartz, T. L., Virgo, K. S., Fischer, L. K., and Brown, J. W., 2007, "Fontan Operation: A Comparison of Lateral Tunnel with Extracardiac Conduit," Ann Thorac Surg, 83, pp. 622–630.

[13] Lee, J. R., Kwak, J. G., Kim, K. J., Min, S. K., Kim, W., Kim, Y. J., and Rhoa, J. R., 2007, "Comparison of lateral tunnel and extracardiac conduit Fontan procedure," Interactive CardioVascular and Thoracic Surgery, 6, pp. 328–330.

[14] Sundareswaran, K. S., Kanter, K. R., Kitajima, H. D., Krishnankutty, R., Sabatier, J. F., Parks, W. J., Sharma, S., Yoganathan, A. P., and Fogel, M., 2006, "Impaired power output and cardiac index with hypoplastic left heart syndrome: a magnetic resonance imaging study," Ann Thorac Surg, 82(4), pp. 1267-1275; discussion 1275-1267.

[15] Whitehead, K., Pekkan, K., Kitajima, H., de Zelicourt, D., Fogel, M., and Yoganathan, A. P., 2007, "Computational Model of Exercise Effects on Fontan Hemodynamics Demonstrates Favorable Energetics in Extracardiac Fontans When Compared to Lateral Tunnel," The American Heart Association (AHA) Scientific Sessions (accepted).

[16] Dasi, L. P., Pekkan, K., Whitehead, K., Fogel, M., and Yoganathan, A. P., 2007, "Hepatic Blood Flow Distribution in the Total Cavopulmonary Connection: Patient-Specific Anatomical Models," ASME 2007 Summer Bioengineering Conference (SBC2007), P. o. t. ASME, ed.Keystone Resort & Conference Center, Keystone, Colorado.

[17] Krishnankuttyrema, R., Dasi, L., Pekkan, K., Sundareswaran, K., Kitajima, H., and Yoganathan, A. P., 2007, "A Unidimensional Representation of the Total Cavopulmonary Connection," ASME 2007 Summer Bioengineering Conference (SBC2007), P. o. t. ASME, ed.Keystone Resort & Conference Center, Keystone, Colorado.

[18] Sundareswaran, K., Fogel, M., Pekkan, K., Kitajima, H., Parks, W., Sharma, S., and Yoganathan, A., 2006, "Viscous Dissipation Power Loss of the Total Cavopulmonary Connection Evaluated Using Phase Contrast Magnetic Resonance Imaging," The American Heart Association (AHA) Scientific SessionsChicago.

[19] Kaulitz, R., and Hofbeck, M., 2005, "Current treatment and prognosis in children with functionally univentricular hearts," Arch. Dis. Child., 90, pp. 757-762.

[20] Norwood, W., and Jacobs, M. L., 1993, "Fontan's Procedure in Two Stages," The American Journal of Surgery, 166, pp. 548-551.

[21] Douglas, W. I., Goldberg, C. S., Mosca, R. S., Law, I. H., and Bove, E. L., 1999, "Hemi-Fontan Procedure for Hypoplastic Left Heart Syndrome: Outcome and Suitability for Fontan," Ann Thorac Surg, 68, pp. 1361– 1368.

[22] Bando, K., Turrentine, M. W., Park, H. J., Sharp, T. G., Scavo, V., and Brown, J. W., 2000, "Evolution of the Fontan Procedure in a Single Center," Ann Thorac Surg, 69(1873–9).

[23] Bove, E. L., de Leval, M. R., Migliavacca, F., Guadagni, G., and Dubini, G., 2003, "Computational fluid dynamics in the evaluation of hemodynamic performance of cavopulmonary connections after the Norwood procedure for hypoplastic left heart syndrome," The Journal of Thoracic and Cardiovascular Surgery, 126(4), pp. 1040-1047.

[24] Degroff, C. G., 2007, "Modeling the Fontan Circulation: Where We Are and Where We Need to Go," Pediatr Cardiol.

[25] Cebral, J. R., Castro, M. A., Burgess, J. E., Pergolizzi, R. S., Sheridan, M. J., and Putman, C. M., 2005, "Characterization of cerebral aneurysms for assessing risk of rupture by using patient-specific computational hemodynamics models," Am. J. Neuroradiol., 26(10), pp. 2550-2559.

[26] Pekkan, K., Whited, B., Kanter, K., Sharma, S., Krishnankutty, R., Sundareswaran, K., Frakes, D., Rossignac, J., and Yoganathan, A. P., 2007, "Patient Specific Surgical Planning and

Hemodynamic Computational Fluid Dynamic Optimization through Free-Form Haptic Anatomy Editing Tool (SURGEM)," Medical & Biological Engineering & Computing, in review

[27] Rossignac, J., Pekkan, K., Whited, B., Kanter, K., Sharma, S., and Yoganathan, A., 2006, "Surgem: Next Generation CAD Tools for Interactive Patient-Specific Surgical Planning and Hemodynamic Analysis," Georgia Institute of Technology, Atlanta.

[28] Pekkan, K., Kitajima, H., Forbess, J., Fogel, M., Kanter, K., Parks, J. M., Sharma, S., and Yoganathan, A. P., 2005, "Total Cavopulmonary Connection Flow with Functional Left Pulmonary Artery Stenosis – Fenestration and Angioplasty in Vitro," Circulation, 112(21), pp. 3264-3271.

[29] Sorensen, T. S., Greil, G. F., Hansen, O. K., and Mosegaard, J., 2006, "Surgical simulation--a new tool to evaluate surgical incisions in congenital heart disease?," Interact Cardiovasc Thorac Surg, 5(5), pp. 536-539.

[30] Magosso, E., Cavalcanti, S., and Ursino, M., 2002, "Theoretical analysis of rest and exercise hemodynamics in patients with total cavopulmonary connection," Am J Physiol Heart Circ Physiol., 282, pp. H1018-H1034.

[31] Mace, L., Dervanian, P., Bourriez, A., Mazmanian, G. M., Lambert, V., and Neveux, J., 2000, "Changes in venous return parameters associated with univentricle Fontan circulations," Am J Physiol Heart Circ Physiol., 279, pp. H2335-H2343.

[32] Pekkan, K., Frakes, D., De Zelicourt, D., Lucas, C. W., Parks, W. J., and Yoganathan, A. P., 2005, "Coupling pediatric ventricle assist devices to the Fontan circulation: simulations with a lumped-parameter model," Asaio J, 51(5), pp. 618-628.

[33] Kelly, J. R., Mack, G. W., and Fahey, J. T., 1995, "Diminished venous vascular capacitance in patients with univentricular hearts after the Fontan operation," Am J Cardiol, 76, pp. 158-163.

[34] Guyton, A. C., ed., 1961, Cardiac output and venous return, and their regulation, Saunders, Philadelphia, PA.

[35] Guyton, A. C., Abernathy, B., Langston, J. B., Kaufmann, B. N., and Fairchild, H. M., 1959, "Relative importance of venous and arterial resistances in controlling venous return and cardiac output," Am J Physiol, 196, pp. 1008-1014.

[36] Sundareswaran, K., Pekkan, K., de Zelicourt, D., Dasi, L. P., Kitajima, H., Whitehead, K., Fogel, M., and Yoganathan, A. P., 2007, "Significant impact of the total cavopulmonary connection (TCPC) resistance on cardiac output and exercise performance in single ventricles," The American Heart Association (AHA) Scientific Sessions (accepted).

[37] Whitehead, K., Pekkan, K., Kitajima, H., Paridon, S., Fogel, M., and Yoganathan, A. P., 2007, "Non-Linear Power Loss During Exercise in Single Ventricle Patients After the Fontan: Insights From Computational Fluid Dynamics," Circulation (Supp I), (in press).

[38] Guyton, A. C., Abernathy, B., Langston, J. B., Kaufmann, B. N., and Fairchild, H. M., 1959, "Relative importance of venous and arterial resistances in controlling venous return and cardiac output," Am J Physiol, 196(5), pp. 1008-1014.

[39] Guyton, A. C., Lindsey, A. W., and Kaufmann, B. N., 1955, "Effect of mean circulatory filling pressure and other peripheral circulatory factors on cardiac output," Am J Physiol, 180(3), pp. 463-468.

[40] Frakes, D. H., Conrad, C. P., Healy, T. M., Monaco, J. W., Fogel, M., Sharma, S., Smith, M. J., and Yoganathan, A. P., 2003, "Application of an adaptive control grid interpolation technique to morphological vascular reconstruction," IEEE Trans Biomed Eng, 50(2), pp. 197-206.

[41] Frakes, D. H., Smith, M. J., Parks, J., Sharma, S., Fogel, S. M., and Yoganathan, A. P., 2005, "New techniques for the reconstruction of complex vascular anatomies from MRI images," J Cardiovasc Magn Reson, 7(2), pp. 425-432.

[42] Frakes, D. H., Dasi, L. P., Pekkan, K., Kitajima, H., Yoganathan, A. P., and Smith, M. J. T., 2007, "A new adaptive method for registration-based medical image interpolation," IEEE Trans Biomed Eng, in press.

[43] Zelicourt, D., Pekkan, K., Kitajima, H., Frakes, D., and Yoganathan, A. P., 2005, "Single-Step Stereolithography of Complex Anatomical Models for Optical Flow Measurements," Journal of Biomechanical Engineering, 127(1), pp. 204-207.

[44] Soerensen, D. D., Pekkan, K., Sundareswaran, K. S., and Yoganathan, A. P., 2004, "New power loss optimized Fontan connection evaluated by calculation of power loss using high resolution PC-MRI and CFD," Conf Proc IEEE Eng Med Biol Soc, 2, pp. 1144-1147.

[45] Frakes, D., Smith, M. J. T., Zelicourt, D., Pekkan, K., and Yoganathan, A. P., 2004, "Three-Dimensional Velocity Field Reconstruction," Journal of Biomechanical Engineering, 126(6), pp. 727-735.

[46] Soerensen, D., Pekkan, K., de Zélicourt, D., Parks, J., Kanter, K., Fogel, M., and Yoganathan, A. P., 2007, "Introduction of a New Optimized Total Cavopulmonary Connection," The Annals of Thoracic Surgery, 83, pp. 2182–2190.

[47] Zélicourt, D., Pekkan, K., Parks, W. J., Kanter, K., Fogel, M., and Yoganathan, A. P., 2006, "Flow study of an extra-cardiac connection with persistent left superior vena cava," The Journal of Thoracic and Cardiovascular Surgery, 131(4), pp. 785-791.

[48] Zelicourt, D., Pekkan, K., Wills, L., Kanter, K. S., S., Fogel, M., and Yoganathan, A. P., 2005, "In Vitro Flow Analysis of a Patient Specific Intra-Atrial TCPC," Annals of Thoracic Surgery, 79(6), pp. 2094-2102.

[49] Pekkan, K., Zelicourt, D., Ge, L., Sotiropoulos, F., Frakes, D., Fogel, M., and P., Y. A., 2005, "Physics-Driven CFD Modeling of Complex Anatomical Cardiovascular Flows—A TCPC Case Study," Annals of Biomedical Engineering, 33(3), pp. 284-300.

[50] Wang, C., Pekkan, K., de Zelicourt, D., Hormer, M., Parihar, A., Kulkarni, A., and Yoganathan, A., 2007, "Progress in the CFD Modeling of Flow Instabilities in Anatomical Total Cavopulmonary Connections," Annals of Biomedical Engineering, in press.

[51] Sundareswaran, K., de Zelicourt, D., Pekkan, K., Jayaprakash, G., Kim, D., Rossignac, J., Fogel, M., Kanter, K., and Yoganathan, A., 2007, "Anatomically Realistic Patient-Specific Surgical Planning of Complex Congenital Heart Defects Using MRI and CFD," 29th IEEE EMBS Annual International ConferenceCité Internationale, Lyon, France.

[52] Ryu, K., Healy, T. M., Ensley, A. E., Sharma, S., Lucas, C., and Yoganathan, A. P., 2001, "Importance of accurate geometry in the study of the total cavopulmonary connection: computational simulations and in vitro experiments," Ann Biomed Eng, 29(10), pp. 844-853.

[53] Ensley, A. E., Ramuzat, A., Healy, T. M., Chatzimavroudis, G. P., Lucas, C., Sharma, S., Pettigrew, R., and Yoganathan, A. P., 2000, "Fluid mechanic assessment of the total cavopulmonary connection using magnetic resonance phase velocity mapping and digital particle image velocimetry," Ann Biomed Eng, 28(10), pp. 1172-1183.

[54] Ensley, A. E., Lynch, P., Chatzimavroudis, G. P., Lucas, C., Sharma, S., and Yoganathan, A. P., 1999, "Toward designing the optimal total cavopulmonary connection: an in vitro study," Ann Thorac Surg, 68(4), pp. 1384-1390.

[55] Hosein, R. B., Clarke, A. J., McGuirk, S. P., Griselli, M., Stumper, O., De Giovanni, J. V., Barron, D. J., and Brawn, W. J., 2007, "Factors influencing early and late outcome following the Fontan procedure in the current era. The 'Two Commandments'?," Eur J Cardiothorac Surg, 31(3), pp. 344-352; discussion 353.

[56] Fogel, M. A., Weinberg, P. M., Rychik, J., Hubbard, A., Jacobs, M., Spray, T. L., and Haselgrove, J., 1999, "Caval contribution to flow in the branch pulmonary arteries of Fontan patients with a novel application of magnetic resonance presaturation pulse," Circulation, 99(9), pp. 1215-1221.

[57] Hirsch, J. C., Ohye, R. G., Devaney, E. J., Goldberg, C. S., and Bove, E. L., 2007, "The Lateral Tunnel Fontan Procedure for Hypoplastic Left Heart Syndrome: Results of 100 Consecutive Patients," Pediatr Cardiol.

[58] Dasi, L., Sundareswaran, K., Zelicourt, D., Krishnankutty, R., Kitajima, H., del Nido, P. J., and Yoganathan, A., 2007, "Proper indexing of Fontan energetics: amended clinical interpretation and a new index for total cavopulmonary

connection hemodynamic efficiency," Circulation, in review.

[59] Masters, J. C., Ketner, M., Bleiweis, M. S., Mill, M., Yoganathan, A., and Lucas, C. L., 2004, "The effect of incorporating vessel compliance in a computational model of blood flow in a total cavopulmonary connection (TCPC) with caval centerline offset," J Biomech Eng, 126(6), pp. 709-713.

[60] Orlando, W., Shandas, R., and DeGroff, C., 2006, "Efficiency differences in computational simulations of the total cavo-pulmonary circulation with and without compliant vessel walls," Comput Methods Programs Biomed, 81(3), pp. 220-227.

List of Figures

Figure 1: Typical three-dimensional patient-specific reconstructions of the hemi- and Glenn type S2R pathway templates. Superior caval offset distance is represented by d. LPA: Left pulmonary artery, RPA: Right pulmonary artery, SVC: Superior vena cava

Figure 2: Photographs of the stereolithographic models used in particle image velocimetry experiments. Only 4 out of the 6 second stage patient specific models that are analyzed are shown in this figure. Left column is Glenn template and Right column is hemi-Fontan.

Figure 3: Idealized 2nd stage models with the geometric dimensions and configurations studied in CFD. (a) Four models are created with varying SVC offset diameter, d as summarized in the Table. Case GL with d = 0 mm approximate the Glenn configuration. Other three models correspond to hemi-Fontan with larger degree of SVC offset. In (b) variable SVC constriction (stenosis) is studied in two models which are created by reducing the SVC anastomosis pathway cross-sectional area in HM-3. (HM-3 model feature the maximum possible superior caval anastomosis area)

Figure 4: Power loss characteristics of the idealized S2R models at different right pulmonary artery splits (% RPA). Superior vena cava (SVC) flow rate is 1.6 LPM for all models. Effect of SVC offset and SVC anastomosis narrowing is compared in (a) and (b) respectively.

Figure 5: Major flow structures in the idealized 2nd stage models. The CFD model is viewed from the inferior direction. (a) Flow swirl structure at the LPA (colors indicate through plane vorticity magnitude, red color: 89 s-1 red color: -47 s-1) (b) SVC jet through the anastomosis. (c) Stagnation region of the SVC jet (d) Pouch vortex. Only the streamlines going to the left lung are plotted for better clarification of the flow structures. Colors of the streamlines correspond to velocity magnitude, red: high velocity (0.5m/s) and blue low velocity (0.03m/s)

Figure 6: CFD and PIV flow-fields along a typical section (registered on the 3D anatomy on the left) computed from CFD and measured using particle image velocimetry (PIV), (a) for the hemi-Fontan and (b) for the Glenn model.

Figure 7: Flow streamlines (LEFT) and pressure distribution (RIGHT) of Glenn models. SVC: Superior vena cava, LPA: Left pulmonary artery, RPA: Right pulmonary artery. Pressures are in mmHg and measured with respect to the LPA outlet. LPA streamlines are marked with alternating colors of blue-green and RPA streamlines are marked with orange-red. Blue arrows indicate major flow structures as discussed in Section 3.3.

Figure 8: Flow streamlines (LEFT) and pressure distribution (RIGHT) of hemi-Fontan models. SVC: Superior vena cava, LPA: Left pulmonary artery, RPA: Right pulmonary artery. Pressures are in mmHg and measured with respect to the LPA outlet. LPA streamlines are marked with alternating colors of blue-green and RPA streamlines are marked with orange-red. Blue arrows indicate major flow structures as discussed in Section 3.3.

Figure 9: Velocity magnitude (m/s) in a typical section of the hemi-Fontan model (Database ID: CHOP036) for three different mesh refinements. COARSE: 133936, MEDIUM: 232036 and FINE: 330555 mesh sizes.

Figure 10: “Virtual” surgeries exploring the effects of anatomical features selectively. LEFT: Glenn model (NIH Database ID: CHOA013) where three PA stenosis are removed (Model C, B

and E), anastomosis is enlarged with a patch (Model A) and RPA flare added (Model E) to the original anatomy. RIGHT: Three virtual modifications performend on the hemi-Fontan anatomy (NIH Database ID: CHOP036) where the pouch size is reduced (Model G) and LPA flare is added (Model H) to the original anatomy.

Figure A1: Effect of extra smoothing on the pressure distribution (mmHg) for a Glenn model (Database ID: CHOA030) Top: is the 3D reconstruction from the standard methodology (For the coronal view please refer to Fig 7). Bottom: Over smoothed model, see arrow. No major differences were apparent in the streamline patterns of these two models.

Figure A2: Effect of distal PA morphology (arrow) on the computed flow fields and pressure drop (mmHg). For the model with a straight PA please refer to Fig 7. (Database ID: Chop057)

List of Tables

Table 1: Converged grid sizes used in the CFD simulations. For typical mesh sizes used sensitivity studies please refer to Sections 3.1 and 3.3.

Table 2: Hemodynamic parameters and power loss for the patient specific anatomical models. Maximum Reynolds number is based on vessel diameter and the corresponding vessel is also indicated in the Table. CHOP053 is a bilateral SVC model with 55/45 LSVC/RSVC flow split and 12.6 mm LSVC hydraulic diameter.

Table 1: Converged grid sizes used in the CFD simulations. For typical mesh sizes used sensitivity studies please refer to Sections 3.1 and 3.3.

	MODEL	ELEMENT NO	NODE NO
Idealized	GL	406186	77626
	HM-1	393313	75513
	HM-2	428760	81330
	HM-3	435632	82738
	HM-4	415339	79378
	HM-5	442727	83981
Patient-specific	CHOP053	623232	285953
	CHOA030	203466	115804
	CHOP057	534223	263390
	CHOP046	318935	175516
	CHOP072	462995	164264
	CHOP036	330555	125704

Table 2: Hemodynamic parameters and power loss for the patient specific anatomical models. Maximum Reynolds number is based on vessel diameter and the corresponding vessel is also indicated in the Table. CHOP053 is a bilateral SVC model with 55/45 LSVC/RSVC flow split and 12.6 mm LSVC hydraulic diameter.

	Model ID	SVC Flow (L/min)	%RPA flow split	Vessel diameters (mm)			Maximum Reynolds number	Connection size ($10 \times mm^3$)	Power Loss (mW)
				LPA	RPA	SVC			
Glenn	CHOP053	0.878	55	10.3	13.9	9.8	243 (RSVC)	441	0.136
	CHOA030	0.788	60	7.8	8.1	13.9	354 (RPA)	1200	0.250
	CHOP057	0.699	60	11.6	15.4	14.7	288 (SVC)	1260	0.044
hemi	CHOP046	0.849	40	6.5	10.7	12.4	475 (LPA)	769	0.622
	CHOP036	1.145	60	6.6	9.2	10.5	664 (SVC)	647	1.450
	CHOP072	0.918	60	15.0	8.4	9.6	371 (SVC)	1050	0.382

Figure1
Click here to download Figure: Figure1.ppt

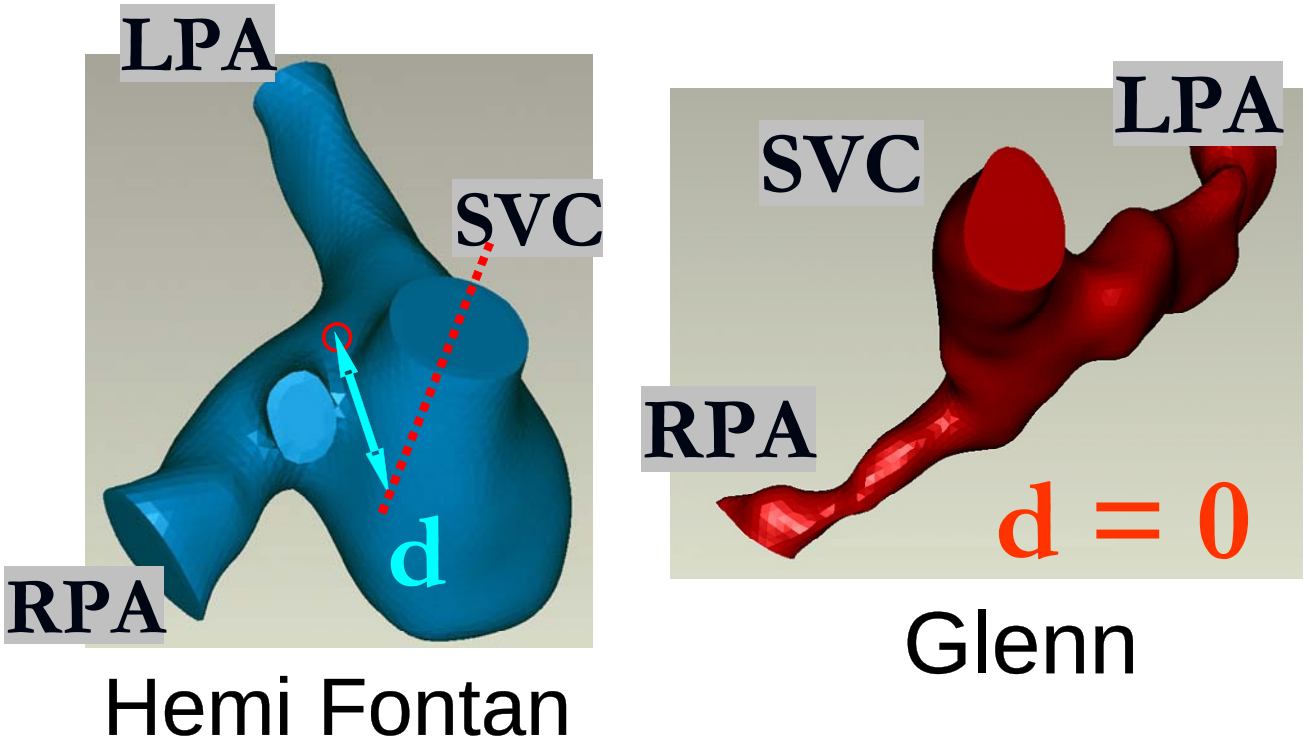

Figure 1: Typical three-dimensional patient-specific reconstructions of the hemi- and Glenn type S2R pathway templates. Superior caval offset distance is represented by d. LPA: Left pulmonary artery, RPA: Right pulmonary artery, SVC: Superior vena cava

Figure2
Click here to download Figure: Figure2.ppt

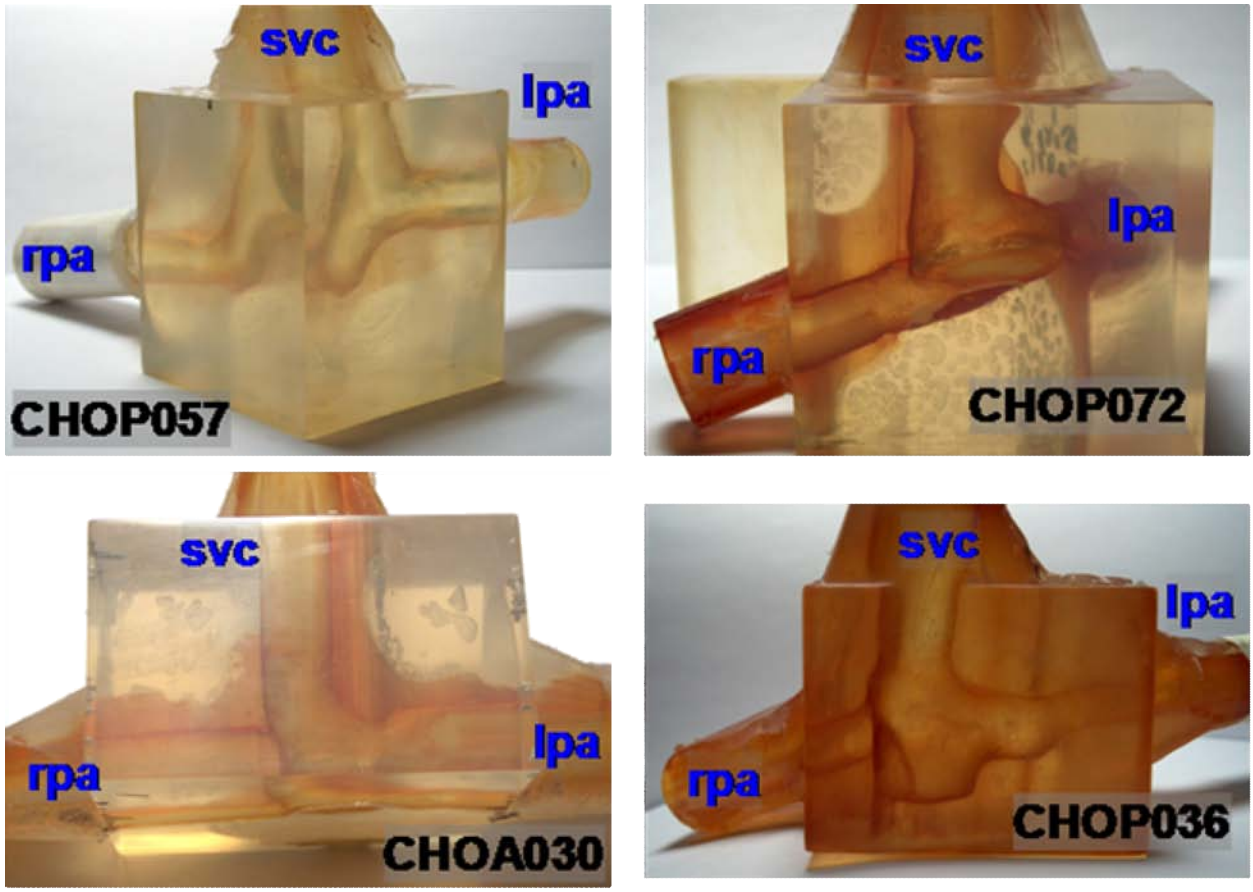

Figure 2: Photographs of the stereolithographic models used in particle image velocimetry experiments. Only 4 out of the 6 second stage patient specific models that are analyzed are shown in this figure. Left column is Glenn template and Right column is hemi-Fontan.

Figure3
Click here to download Figure: Figure3.ppt

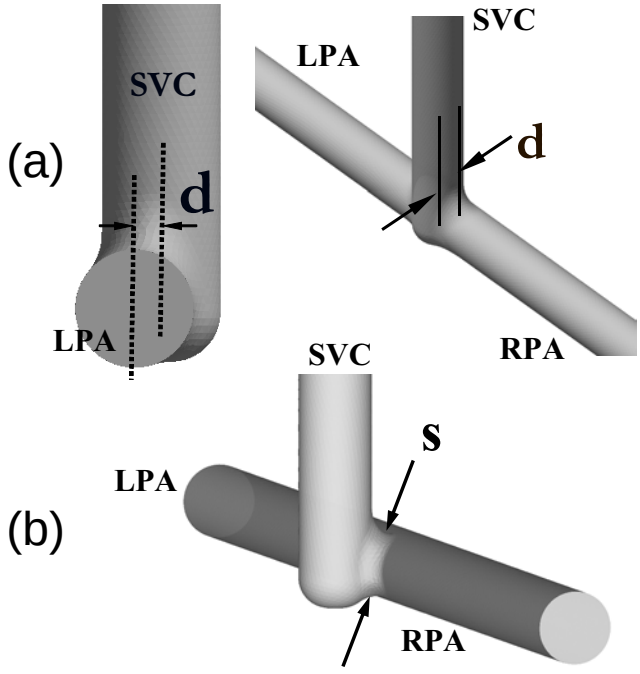

MODEL	d (mm)
GL	0
HM-1	6.6675
HM-2	9.5
HM-3	13.335

MODEL	s (mm)
HM-4	10
HM-5	6

Figure 3: Idealized 2nd stage models with the geometric dimensions and configurations studied in CFD. (a) Four models are created with varying SVC offset diameter, d as summarized in the Table. Case GL with d = 0 mm approximate the Glenn configuration. Other three models correspond to hemi-Fontan with larger degree of SVC offset. In (b) variable SVC constriction (stenosis) is studied in two models which are created by reducing the SVC anastomosis pathway cross-sectional area in HM-3. (HM-3 model feature the maximum possible superior caval anastomosis area)

Figure4
Click here to download Figure: Figure4.ppt

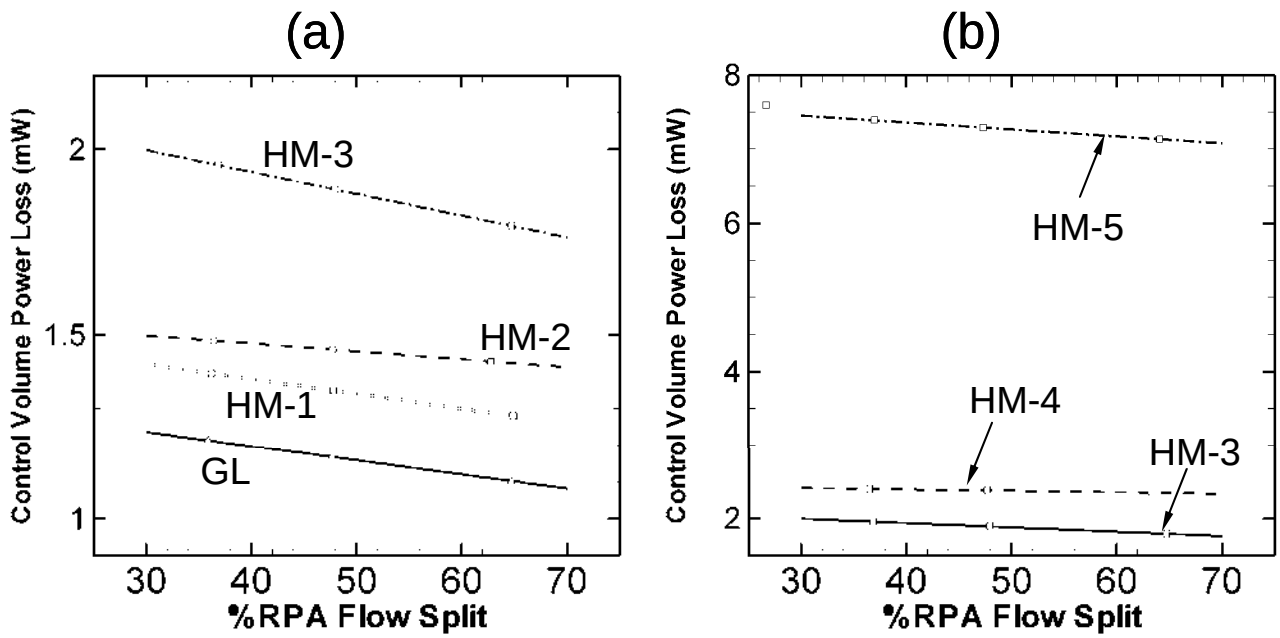

Figure 4: Power loss characteristics of the idealized S2R models at different right pulmonary artery splits (% RPA). Superior vena cava (SVC) flow rate is 1.6 LPM for all models. Effect of SVC offset and SVC anastomosis narrowing is compared in (a) and (b) respectively.

Figure5
Click here to download Figure: Figure5.ppt

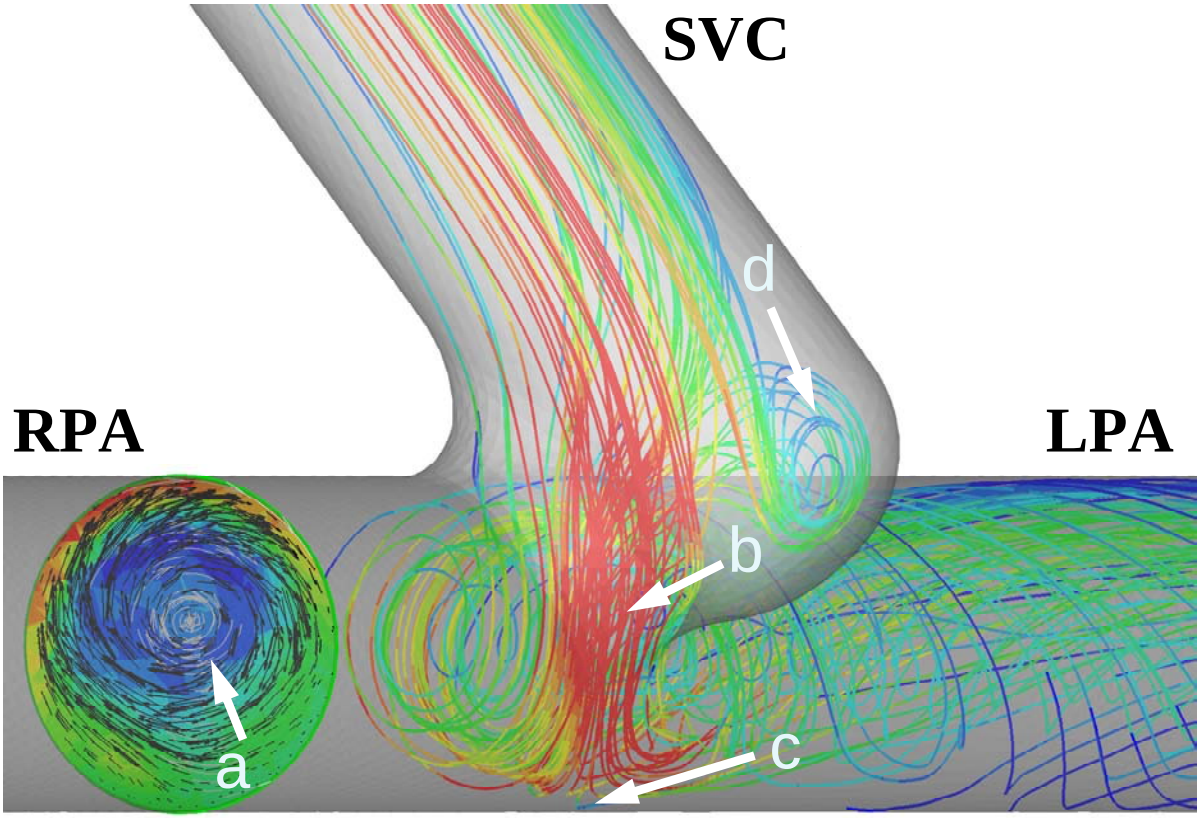

Figure 5: Major flow structures in the idealized 2nd stage models. The CFD model is viewed from the inferior direction. (a) Flow swirl structure at the LPA (colors indicate through plane vorticity magnitude, red color: 89 s^{-1} red color: -47 s^{-1}) (b) SVC jet through the anastomosis. (c) Stagnation region of the SVC jet (d) Pouch vortex. Only the streamlines going to the left lung are plotted for better clarification of the flow structures. Colors of the streamlines correspond to velocity magnitude, red: high velocity (0.5m/s) and blue low velocity (0.03m/s)

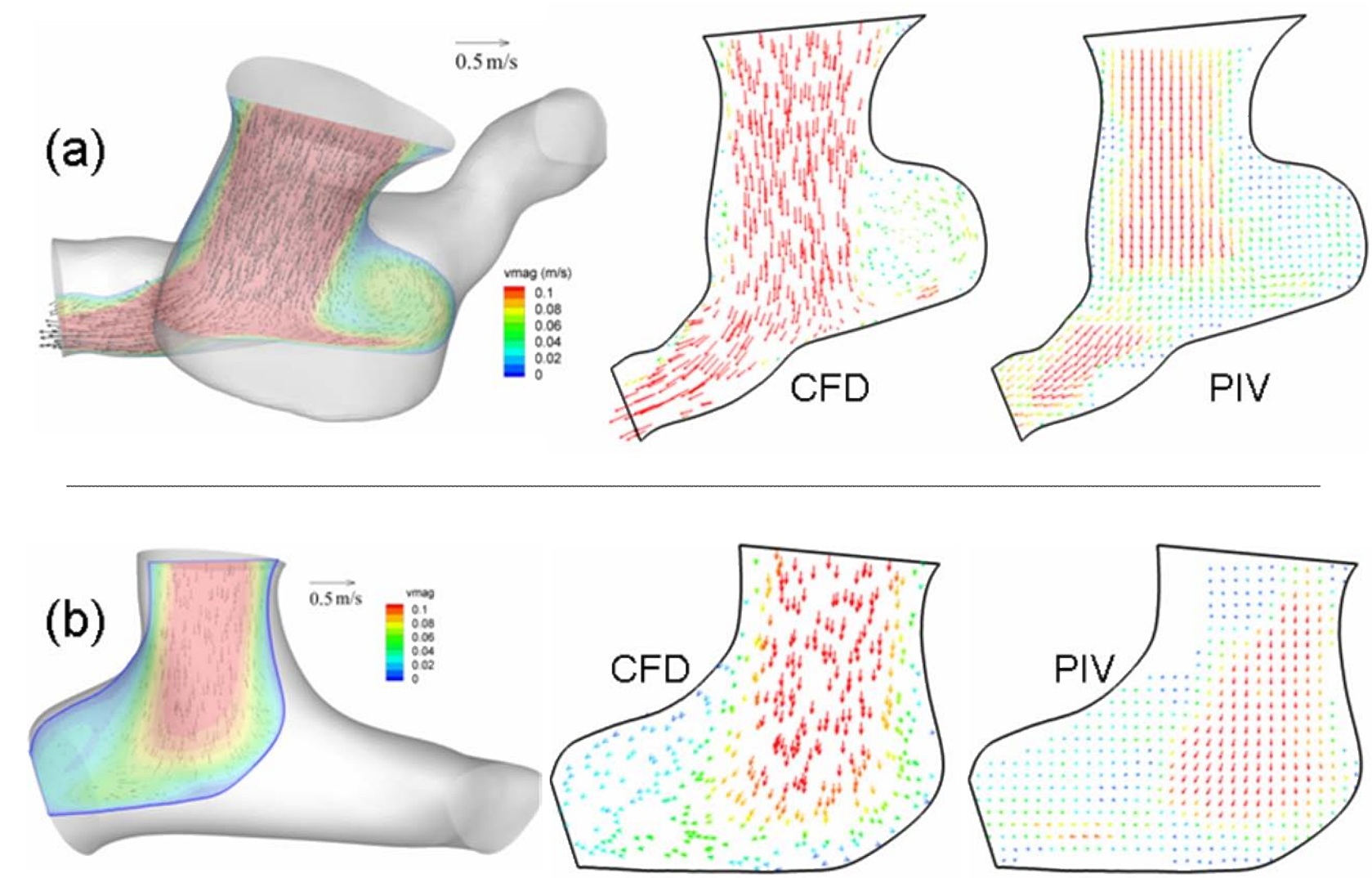

Figure 6: CFD and PIV flow-fields along a typical section (registered on the 3D anatomy on the left) computed from CFD and measured using particle image velocimetry (PIV), (a) for the hemi-Fontan and (b) for the Glenn model.

Figure7
Click here to download Figure: Figure7.ppt

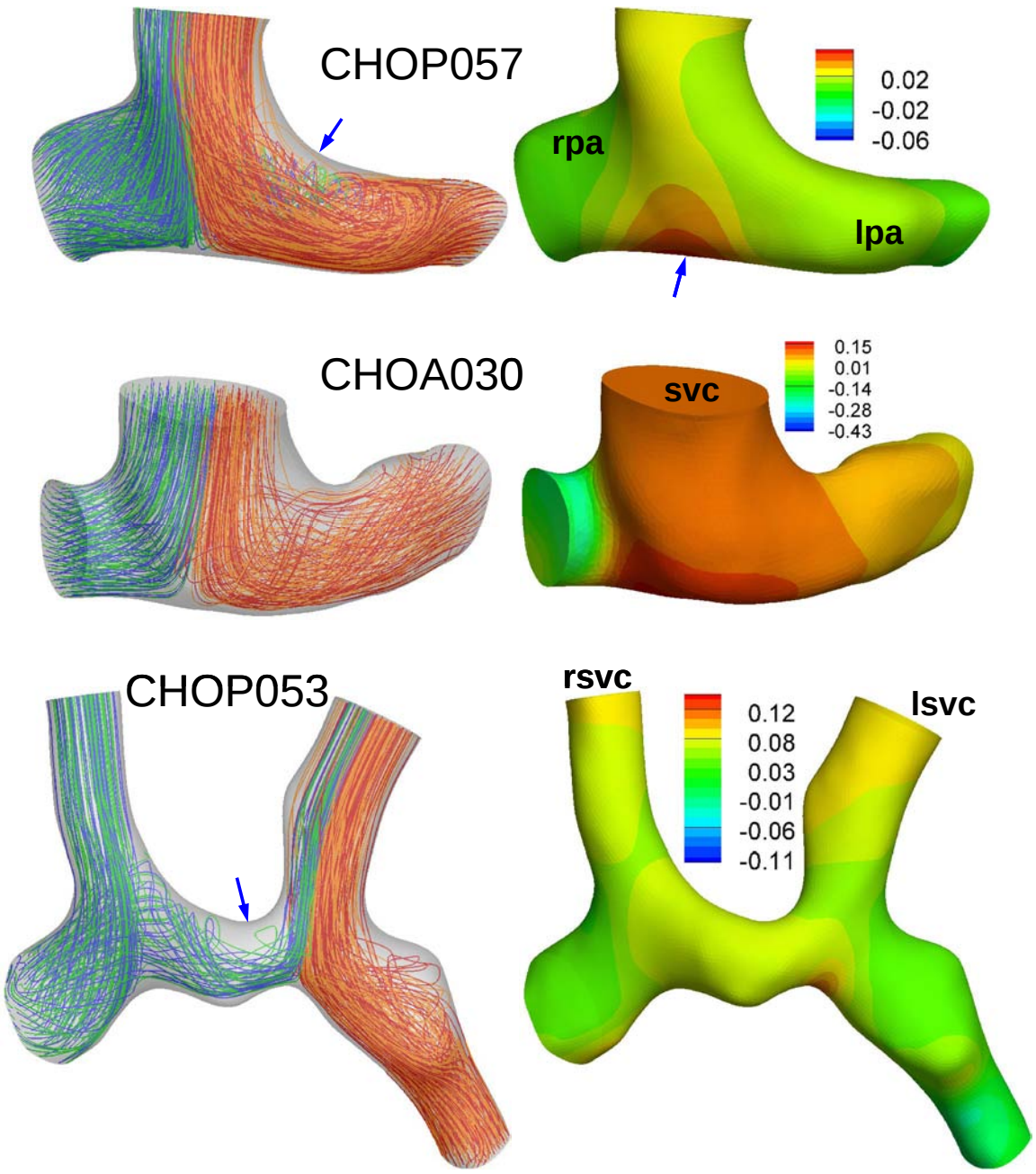

Figure 7: Flow streamlines (LEFT) and pressure distribution (RIGHT) of Glenn models. SVC: Superior vena cava, LPA: Left pulmonary artery, RPA: Right pulmonary artery. Pressures are in mmHg and measured with respect to the LPA outlet. LPA streamlines are marked with alternating colors of blue-green and RPA streamlines are marked with orange-red. Blue arrows indicate major flow structures as discussed in Section 3.3.

Figure8
Click here to download Figure: Figure8.ppt

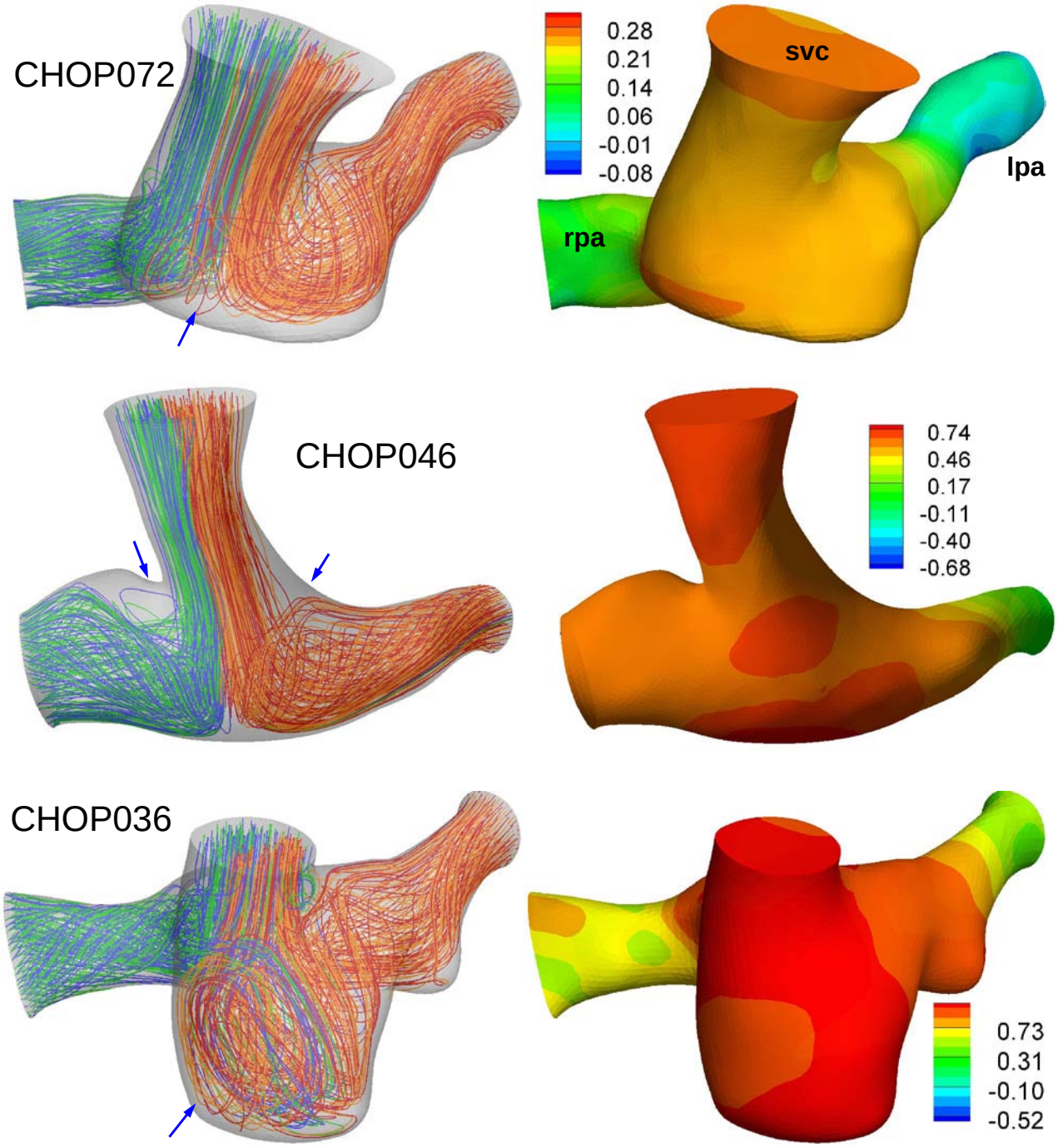

Figure 8: Flow streamlines (LEFT) and pressure distribution (RIGHT) of hemi-Fontan models. SVC: Superior vena cava, LPA: Left pulmonary artery, RPA: Right pulmonary artery. Pressures are in mmHg and measured with respect to the LPA outlet. LPA streamlines are marked with alternating colors of blue-green and RPA streamlines are marked with orange-red. Blue arrows indicate major flow structures as discussed in Section 3.3.

Figure9
Click here to download Figure: Figure9.ppt

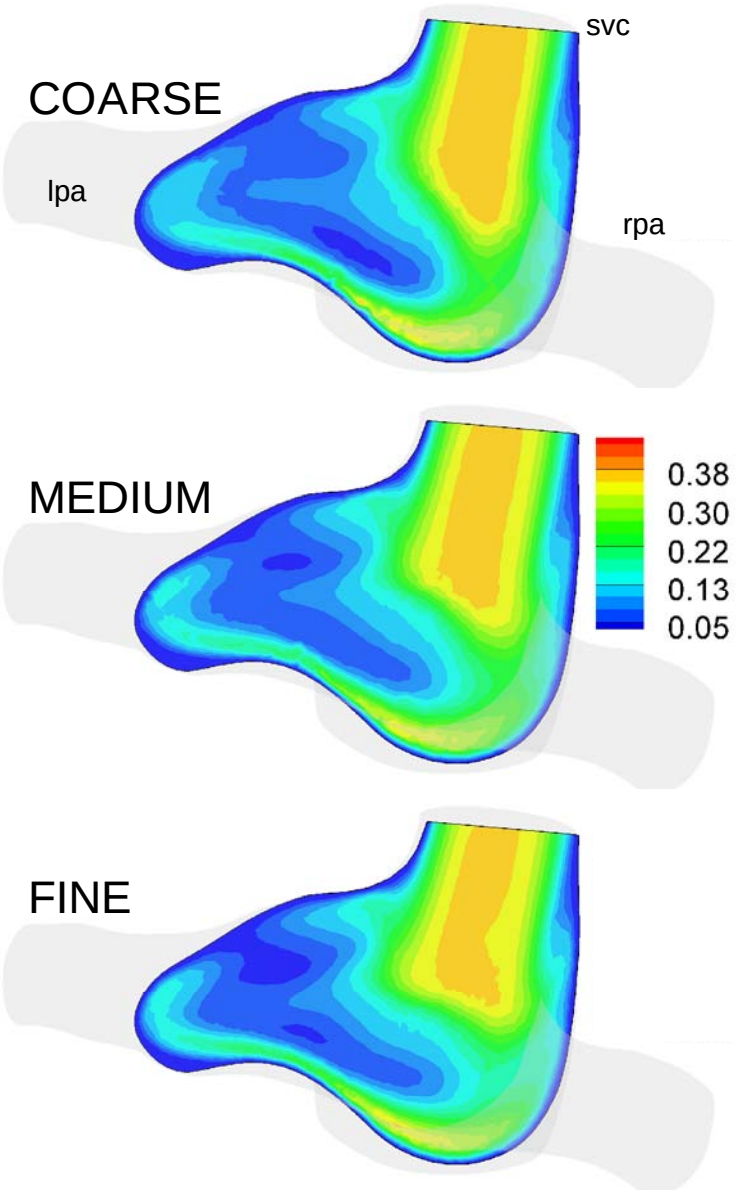

Figure 9: Velocity magnitude (m/s) in a typical section of the hemi-Fontan model (Database ID: CHOP036) for three different mesh refinements. COARSE: 133936, MEDIUM: 232036 and FINE: 330555 mesh sizes.

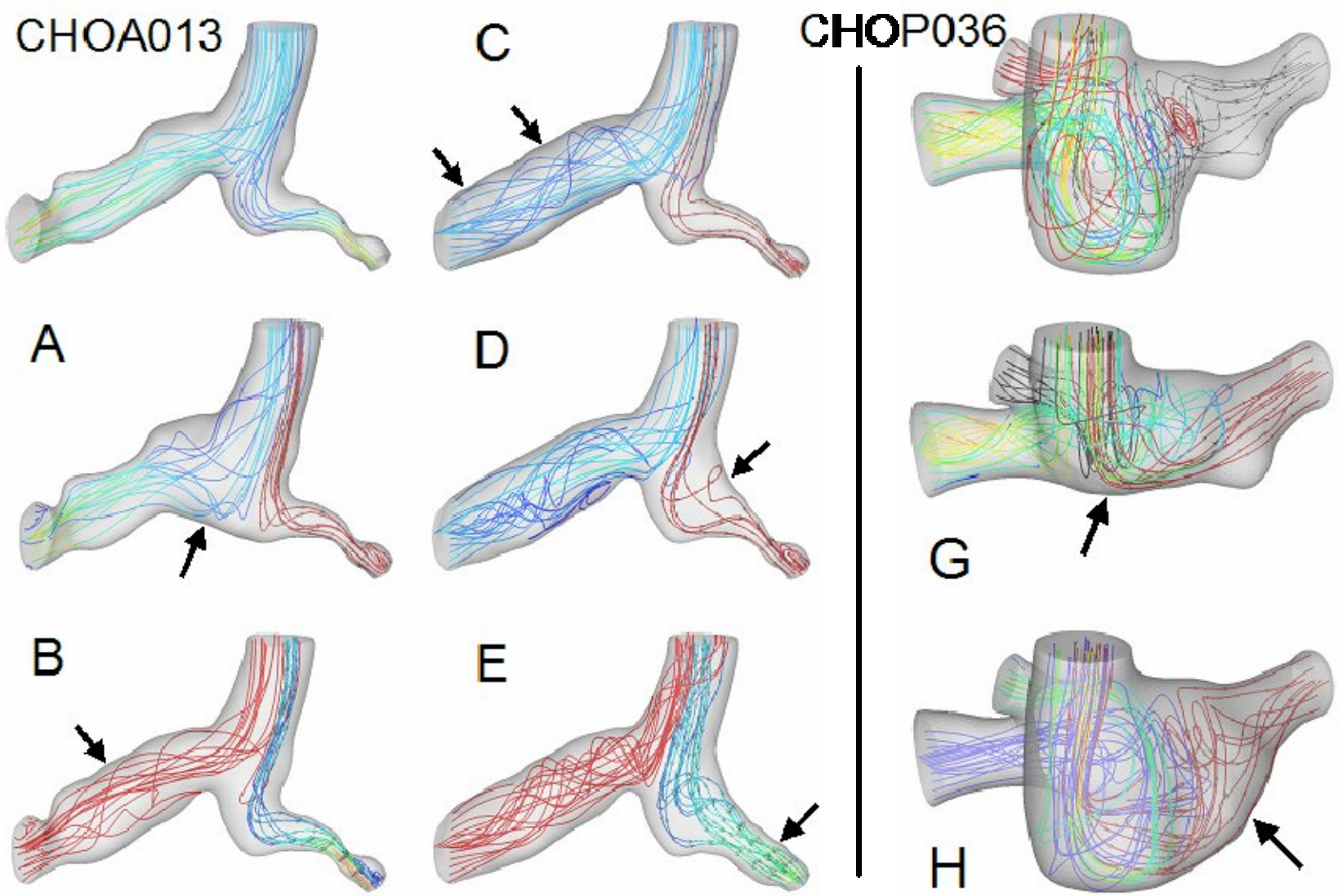

Figure 10: “Virtual” surgeries exploring the effects of anatomical features selectively. LEFT: Glenn model (NIH Database ID: CHOA013) where three PA stenosis are removed (Model C, B and E), anastomosis is enlarged with a patch (Model A) and RPA flare added (Model E) to the original anatomy. RIGHT: Three virtual modifications performend on the hemi-Fontan anatomy (NIH Database ID: CHOP036) where the pouch size is reduced (Model G) and LPA flare is added (Model H) to the original anatomy.

Appendix-FigureA1
Click here to download Figure: FigureA1.ppt

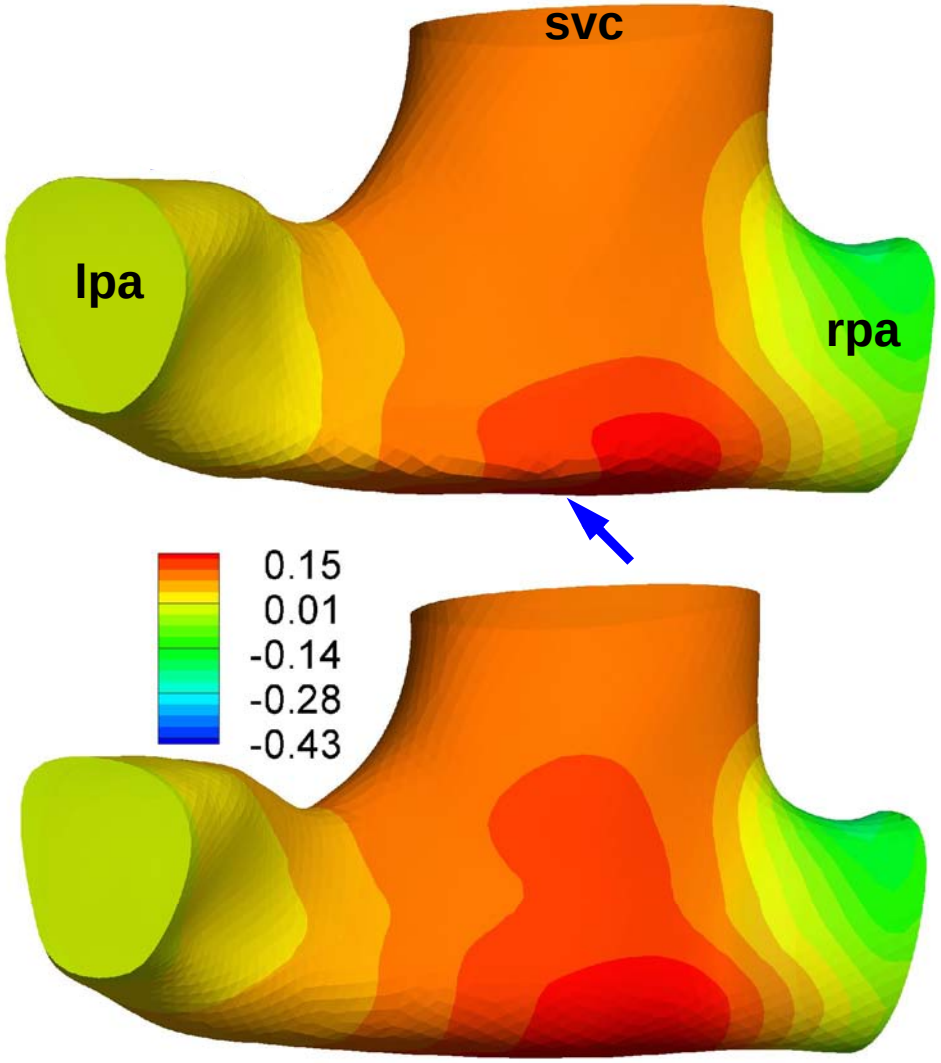

Figure A1: Effect of extra smoothing on the pressure distribution (mmHg) for a Glenn model (Database ID: CHOA030) Top: is the 3D reconstruction from the standard methodology (For the coronal view please refer to Fig 7). Bottom: Over smoothed model, see arrow. No major differences were apparent in the streamline patterns of these two models.

Appendix-FigureA2
Click here to download Figure: FigureA2.ppt

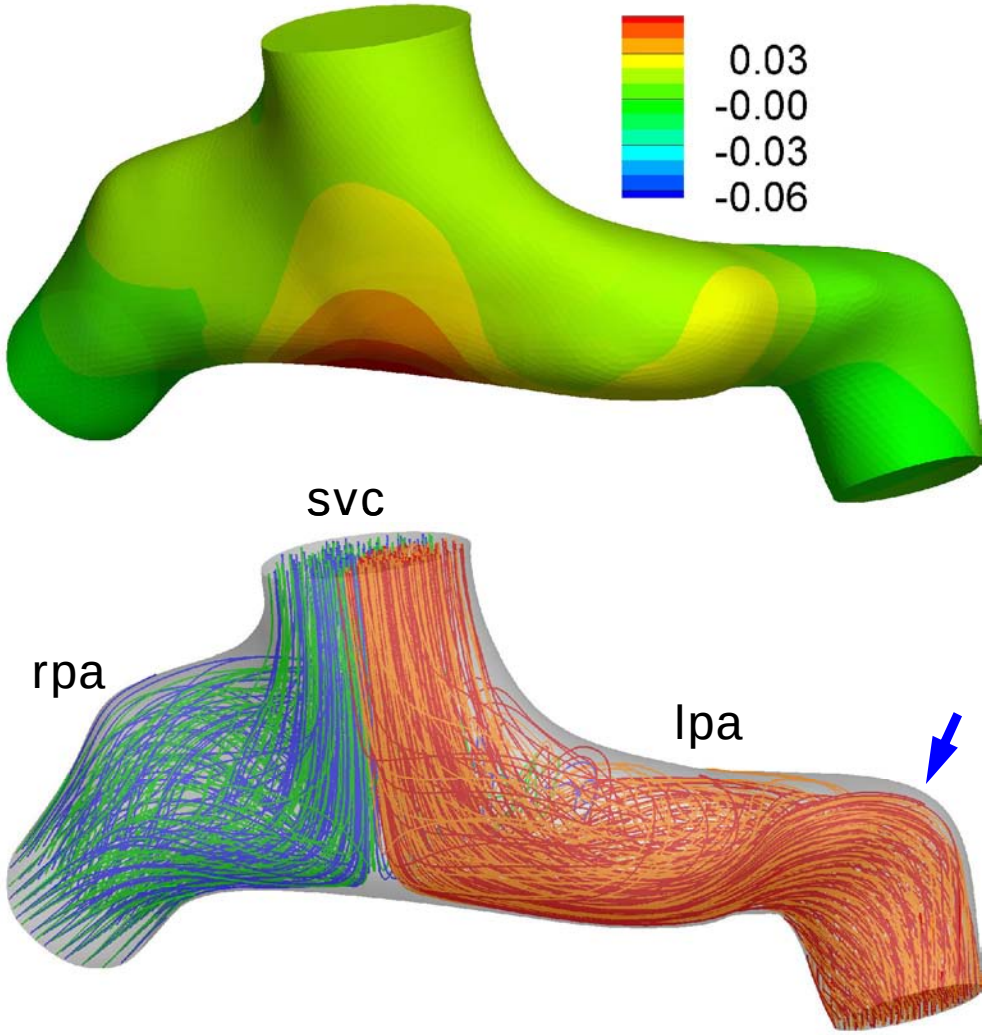

Figure A2: Effect of distal PA morphology (arrow) on the computed flow fields and pressure drop (mmHg). For the model with a straight LPA please refer to Fig 7. (Database ID: Chop057)